

# Parameter sensitivity of a 2D finite volume hydrodynamic model and its application to tsunami simulation

Paul Guard

*BMT WBM, Brisbane, Australia. Email [paul.guard@bmtwbm.com.au](mailto:paul.guard@bmtwbm.com.au)*

Chris Nielsen

*BMT WBM, Brisbane, Australia. Email [chris.nielsen@bmtwbm.com](mailto:chris.nielsen@bmtwbm.com)*

Phil Ryan

*BMT WBM, Brisbane, Australia. Email [phillip.ryan@bmtwbm.com.au](mailto:phillip.ryan@bmtwbm.com.au)*

Ian Teakle

*BMT WBM, Brisbane, Australia. Email [ian.teakle@bmtwbm.com.au](mailto:ian.teakle@bmtwbm.com.au)*

Nobuto Moriya

*Japan Institute of Wastewater Engineering and Technology, Tokyo, Japan. Email [jiwet@jiwet.or.jp](mailto:jiwet@jiwet.or.jp)*

Takefumi Kobayashi

*Nihon Suiko Sekkei Co. Ltd, Tokyo, Japan. Email [t-kobayashi3@n-suiko.co.jp](mailto:t-kobayashi3@n-suiko.co.jp)*

**ABSTRACT:** A two dimensional finite volume hydrodynamic numerical model that solves the non-linear shallow water equations on an unstructured grid (xpswmm2D, using the TUFLOW FV solver) has been applied to simulate the landward propagation and subsequent overland inundation of a tsunami event at a test site in Japan, following the Great East Japan Earthquake in 2011. The model development required an extensive benchmarking and testing process to establish a suitably accurate spatial and temporal model domain and also a suitably accurate numerical scheme which could operate at practical scales and simulation times. The paper discusses the process undertaken to establish model suitability, sensitivity of model performance to spatial resolution and numerical parameters, and its application to further analyses.

**KEY WORDS:** Tsunami, hydrodynamics, finite volume, xpswmm2D, TUFLOW.

## 1 INTRODUCTION

Long wave hydrodynamic numerical models with capacity to simulate wetting and drying provide a means to investigating the landward propagation of a tsunami event, from an initial water level disturbance, over large spatial scales and with reasonable spatial resolution and computational timeframes. Such capabilities provide a means to inform design of coastal infrastructure and management of emergency response on regional, national and global scales.

The Japan Institute of Wastewater Engineering and Technology Manual (JIWET, 2013, also see Acknowledgements) tested a number of numerical engines to assess sensitivity of prediction of tsunami propagation, from an initial water disturbance, with the intention of simulating subsequent peak water levels and overland inundation at the coast. As part of this broader investigation a numerical model called xpswmm2D (XP Solutions, 2013) was considered. xpswmm2D can apply the TUFLOW FV computational engine (BMT 2013a and BMT 2013b), which is a two dimensional long wave finite volume hydrodynamic numerical model.

In order to establish the performance of TUFLOW FV for this purpose, benchmark tests were performed; the initial value problem from Carrier et al (2003) and the Monai Valley physical model from Liu et al (2008). Model predictions were then compared to measurements from the Great East Japan Earthquake event in 2011. The information used to establish this model test was provided by the broader investigation (JIWET, 2013), which defined the extent of the model domain, the baseline bathymetry and topography and characteristics of the initial water level disturbance. The parameter sensitivities

subsequently identified were then submitted to JIWET and will form a component of future studies.

## 2 XPSWMM2D AND TUFLOW FV

### 2.1 Governing Equations

The TUFLOW FV numerical model engine solves the conservative integral form of the non-linear shallow water equations (NLSWE), including viscous flux terms and source terms for Coriolis force, bottom-friction and various surface and volume stresses, on a flexible mesh comprised of triangular and quadrilateral elements. For the present application a two-dimensional approach (2D, with depth averaged velocities through the water column) was adopted.

The 2D NLSWE in conservative integral form solved by TUFLOW FV is:

$$\frac{\partial}{\partial t} \int_{\Omega} \mathbf{U} d\Omega + \oint_{\partial\Omega} (\mathbf{F} \cdot \mathbf{n}) ds = \int_{\Omega} \mathbf{S}(\mathbf{U}) d\Omega \quad (1)$$

where:

- $\mathbf{U} = (h, hu, hv)^T$  is the vector of conserved variables (mass, x- and y-momentum terms)
- $\mathbf{n}$  = the cell-edge (face) unit normal vector
- $\mathbf{E} = (F, G)^T$  represents face fluxes where F and G are the x and y direction flux vectors:

$$\mathbf{F} = \left( hu, hu^2 + gh^2/2, huv \right)^T \quad (2)$$

$$\mathbf{G} = \left( hu, huv, hv^2 + gh^2/2 \right)^T \quad (3)$$

- $\mathbf{S}$  = the standard source term vector:

$$\mathbf{S} = \left( 0, gh \left( \frac{\partial z_b}{\partial x} + S_{fx} \right), gh \left( \frac{\partial z_b}{\partial y} + S_{fy} \right) \right)^T \quad (4)$$

- $h$  = the water depth
- $g$  = acceleration due to gravity
- $u, v$  = the depth averaged components of the velocity vector
- $z_b$  = the bed elevation
- $S_{fx}, S_{fy}$  = the friction slope components
- $\int_{\Omega} d\Omega$  = the cell volume integral
- $\oint_{\partial\Omega} ds$  = the cell surface integral

### 2.2 Solution Scheme

The spatial domain is discretized using contiguous, non-overlapping triangular and quadrilateral cells (or elements). This irregular, flexible mesh approach has significant benefits when applied to study areas involving complex coastlines and embayments, varying bathymetries and sharply varying flow and scalar concentration gradients.

A cell-centered spatial discretization is adopted for all NLSWE conserved variables. The discrete form of the equations for cell  $i$ , with  $k = 1, N_k$  cell-faces is:

$$\frac{\partial \mathbf{U}_i}{\partial t} = -\frac{1}{A_i} \sum_{k=1}^{N_k} (\mathbf{F}_k \cdot \mathbf{n}_k) L_k + \mathbf{S}_i \quad (5)$$

In this discrete equation  $\mathbf{U}_i$  represents the volume-average of the conserved variables in cell  $i$ ,  $A_i$  is the cross-sectional (plan) area of the cell and  $\mathbf{S}_i$  is the volume-averaged source term/s. A first-order midpoint quadrature is used to evaluate the cell boundary flux integral, where  $\mathbf{n}_k$  is the boundary/face unit normal vector for face  $k$  and  $L_k$  is the corresponding face length. The discrete conserved variable field is assumed to be continuous within a cell but discontinuous at the cell-faces.

Non-viscous boundary fluxes are calculated using Roe's approximate Riemann solver. The source

terms due to bed elevation changes between adjacent cells are “up-winded” as part of the Roe flux solver, in order to maintain numerical consistency with the pressure gradient momentum flux terms (Roe, 1981).

Viscous flux terms are calculated using the traditional gradient-diffusion model with a variety of options available for the calculation of eddy-viscosity and scalar diffusivity. The Smagorinsky (Pope, 2000) eddy-viscosity model is most commonly adopted.

### 2.3 Spatial Order

Both first order and second order spatial discretization schemes are available in TUFLOW FV. The first order scheme assumes a piecewise constant value of each conservative constituent in a model cell. The second order scheme assumes a polynomial reconstruction of the conservative constituents within the cell (i.e. a MUSCL scheme). The Total Variation Diminishing (TVD) property is ensured using a choice of gradient limiter schemes, as listed in Table 1.

A higher spatial order can significantly reduce numerical diffusion and provide sharper resolution of gradients in applications where the physical system being solved includes large spatial gradients relative to the discrete mesh size. Numerical diffusion can also be reduced through selection of a finer mesh resolution, however the higher spatial order schemes will generally achieve this outcome with less increase in computational overhead. In general, the solution will benefit from higher spatial order when spatial gradients are sufficiently large relative to the mesh size, though care must be exercised with the higher order solutions to ensure that spurious “overshoots” at the cell faces are avoided by the reconstruction procedure.

The Total Variation Diminishing (TVD) property (and hence stability) of the higher-order scheme solution is achieved using a choice of gradient limiter schemes. A variety of horizontal gradient limiters are available in TUFLOW FV and are listed in Table 1 in order from least to most “compressive”. The most “compressive” schemes will maximize the resolution of sharp gradients but may do so at the expense of additional computational overhead. The most compressive gradient limiter schemes also increase the risk of generating spurious “overshoots” within the solution.

Tsunami typically have a relatively short wave length and steep gradients in the shallow water depths approaching the coastline; in such situations a higher order spatial discretization scheme is expected to provide a better solution compared to first order.

**Table 1** Second Order Horizontal Gradient Limiter Schemes

	Horizontal gradient limiter scheme
Least Compressive	Limited Central Difference (LCD)
↓	Batten et al. (1996)
Most Compressive	Maximum Limited Gradient (MLG)
	Batten et al. (1996)

### 2.4 Time Integration

Temporal integration is performed with an explicit Euler scheme, with timestep bounded by the Courant-Friedrich-Levy (CFL) criterion. A variable timestep scheme is implemented to optimize computational performance.

### 2.5 Wetting and Drying

TUFLOW FV is particularly suited to modelling moving wet-dry boundaries. In very shallow regions (~<0.05m depth) the momentum terms are dropped in order to maintain stability as the NLSWE approach the zero-depth singularity. Mass conservation is maintained both locally and globally to the limit of numerical precision across the entire numerical domain, including wetting and drying fronts. A conservative mass redistribution scheme is used to ensure that negative depths are avoided at numerically challenging wetting and drying fronts without recourse to adjusting the timestep (Murillo et al, 2006). Regions of the model domain that are effectively dry are readily dropped from the computations. Mixed sub/super-critical flow regimes are well handled by the FV scheme which intrinsically accounts for flow discontinuities such as hydraulic jumps or bores that may occur in trans-critical flows.

### 2.6 Initial and Boundary Conditions

TUFLOW FV accommodates a wide variety of initial and boundary conditions including water level time series, in/out flow time series, bed friction, Coriolis force, mean sea level pressure gradients, wind stress and wave radiation stress, available for input using a range of commonly used file formats. For investigations of tsunami propagation from an initial water level disturbance, a spatial initial water level condition and non-reflecting boundary conditions are typically specified.

### 2.7 Multi-core processing

TUFLOW FV is parallelized for multi-processor machines using the OpenMP implementation of shared memory parallelism. This feature has been utilized for the application described herein.

## 3 MODEL APPLICATION TO TSUNAMI

The National Oceanic and Atmospheric Administration (NOAA) has developed a set of procedures for evaluation of numerical models for use in tsunami modelling applications (Synolakis et al, 2007). These procedures include benchmark tests developed as part of the Third International Workshop on Long Wave Run-up Models (Liu et al, 2008). The performance of the TUFLOW FV model has been assessed for two of these benchmark cases. The third case described here is the application to the test site in Japan.

### 3.1 Carrier et al (2003) Initial Value Problem

This analytical problem has an initial offshore water surface profile on a uniform 1:10 slope (Figure 1). The initial water velocity throughout the domain is zero. The initial-value-problem (IVP) technique introduced by Carrier et al (2003) is used to produce the benchmark data. The benchmark task is to produce snapshots of the free surface and velocity profiles at  $t = 160s$ ,  $175s$ , and  $220s$ . Three TUFLOW FV simulations were compared to the benchmark tests:

1. A first order spatial scheme
2. A second order spatial scheme, using the LCD gradient limiter
3. A second order spatial scheme, using the MLG gradient limiter

Comparisons of water level profiles at three different times during the simulation are shown in Figure 2. The results indicate that all three TUFLOW FV simulations are replicating the benchmark solution, however the sharper resolution of the water surface gradients achieved using the second order schemes (simulations 2 and 3) provide a closer match.

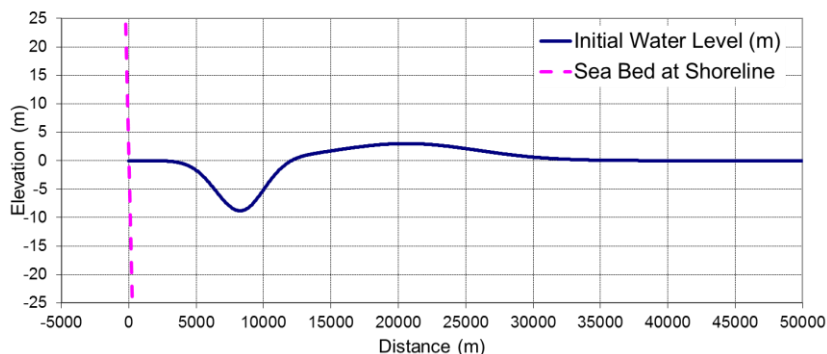


**Figure 1** The Initial Value Problem from Carrier et al (2003), showing the initial water level at time = 0s and bed profile at the shoreline.

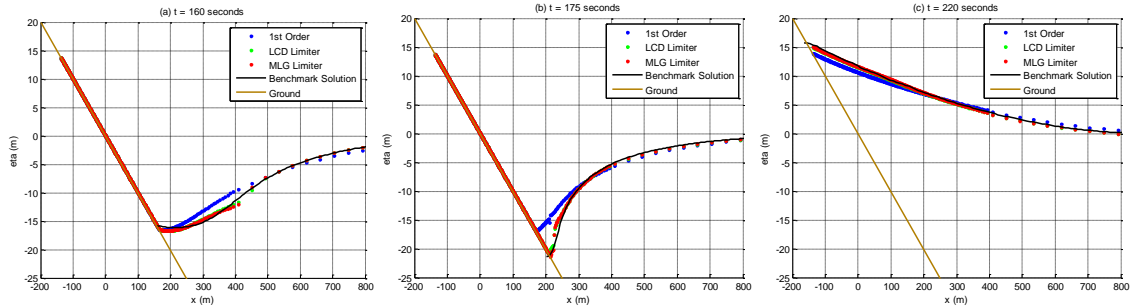


**Figure 2** The Initial Value Problem from Carrier et al (2003), showing profiles of water surface elevation approaching the shoreline at time = 160s (a), 175s (b) and 220 s (c).

### 3.2 Monai Valley, Okushiri Island

The 1993 Okushiri tsunami caused a runup of 32m near the village of Monai in Okushiri Island. This tsunami runup mark was discovered at the tip of a very narrow gulley within a small cove. This benchmark problem is a 1/400 scale laboratory experiment of the Monai runup event that used a large scale tank (205m long, 6m deep, and 3.4m wide). The benchmark task is to reproduce the results of the laboratory experiment documented in Liu et al (2008). Figure 3 shows the bathymetry and coastal topography used in the laboratory experiment and the time series of water level applied at the offshore boundary. The other three boundaries are reflective sidewalls. Three TUFLOW FV simulations were compared to the benchmark tests:

1. A first order spatial scheme
2. A second order spatial scheme, using the LCD gradient limiter
3. A second order spatial scheme, using the MLG gradient limiter

Results from the simulations are compared to the physical model results:

1. Time series of water levels at output locations ch5, ch7 and ch9 (Figure 4, locations shown in Figure 3)
2. A comparison of spatial extent of inundation (Figure 5)

The results demonstrate that all three TUFLOW FV simulations accurately represent the laboratory experiment results. Results from the three different spatial schemes are similar.

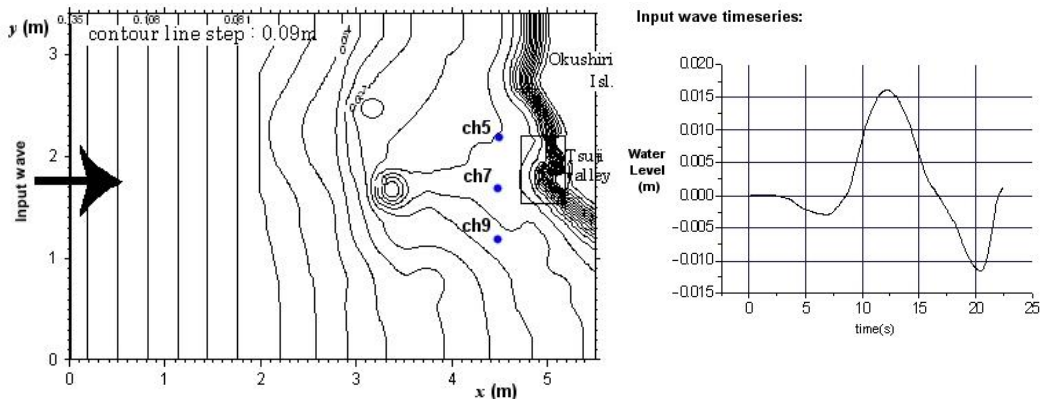


**Figure 3** The laboratory experiment layout (left) and open boundary water level condition (right) for the Monai Valley physical model benchmark test from Liu (2008).

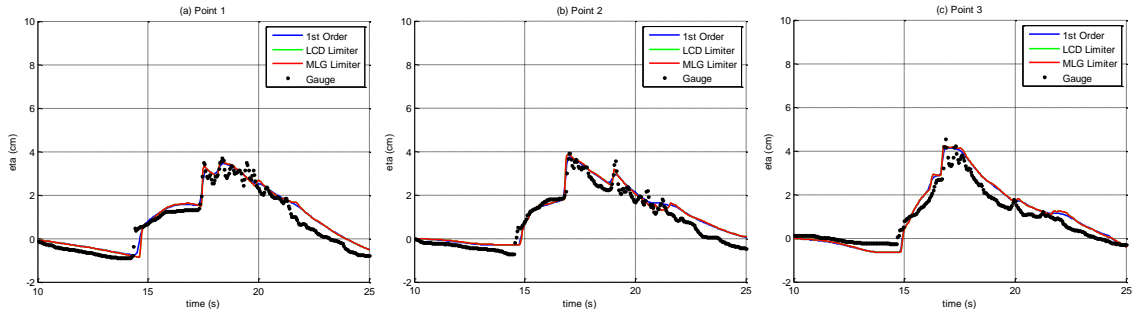


**Figure 4** Time series of water levels at output locations ch5 (left), ch7 (middle) and ch9 (right) for the Monai Valley physical model benchmark test from Liu et al (2008).

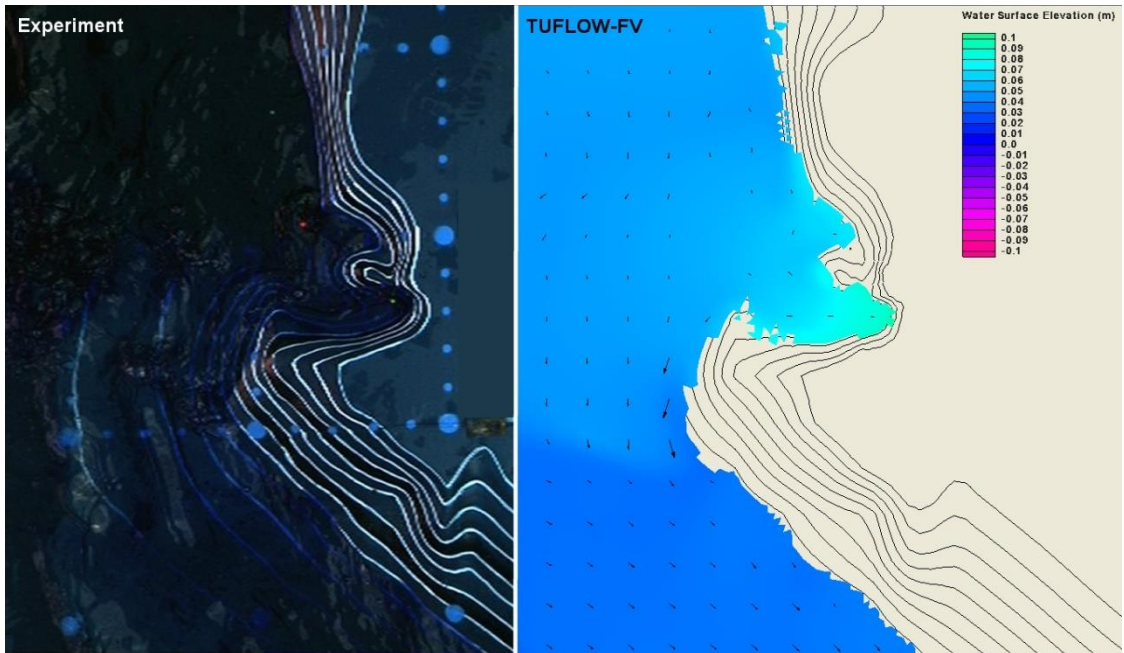


**Figure 5** Comparison of spatial extent of water surface at time 17.1s from a video snapshot from the laboratory experiment (left) and the TUFLOW FV model result (simulation 1, right), from the Monai Valley physical model benchmark test from Liu (2008).

### 3.3 The Great East Japan Earthquake, 2011

The test site is located on the east coast of Japan (Figure 6) and is intended to predict tsunami propagation from an initial water level disturbance to the coastal zone and inland areas.

Tsunami propagation is from an initial water level condition situated approximately 250km offshore (JIWET / NSS, in pub., JIWET, 2013). This has a leading depression of minimum water level  $-4.73\text{m}$  then a following crest of maximum water level  $+15.67\text{m}$  (range  $20.4\text{m}$ , see Figure 6). Initial velocity and momentum terms are set to 0. The model simulation is two hours “real time”, with the tsunami wave reaching the shoreline after approximately 70 minutes.

To optimize computational efficiency a variable mesh resolution is applied (Figure 6 and Table 2), with larger elements in deep water (of the order of  $10\text{km}$  face length) and progressively smaller elements approaching the shoreline and the areas of interest (a minimum  $5\text{m}$  face length).

Five different model meshes with varying mesh resolutions in the vicinity of the initial water level disturbance and subsequent propagation zone into the coastline were sensitivity tested (Table 3). Three spatial order schemes were considered for each mesh resolution:

1. A first order spatial scheme, applying a CFL timestep limiting condition = 1.0
2. A second order spatial scheme, using the LCD gradient limiter, applying a CFL timestep

limiting condition = 0.3

3. A second order spatial scheme, using the MLG gradient limiter, applying a CFL timestep limiting condition = 0.3

Simulation times are shown in Table 2. Application of a CFL timestep limiting criteria of 0.3 for the second order scheme, which results in a longer computation, is in line with the theoretical numerical stability limit (Murillo et al., 2007). Simulations using the MLG limiter were around 60% longer than the equivalent simulations using the LCD limiter.

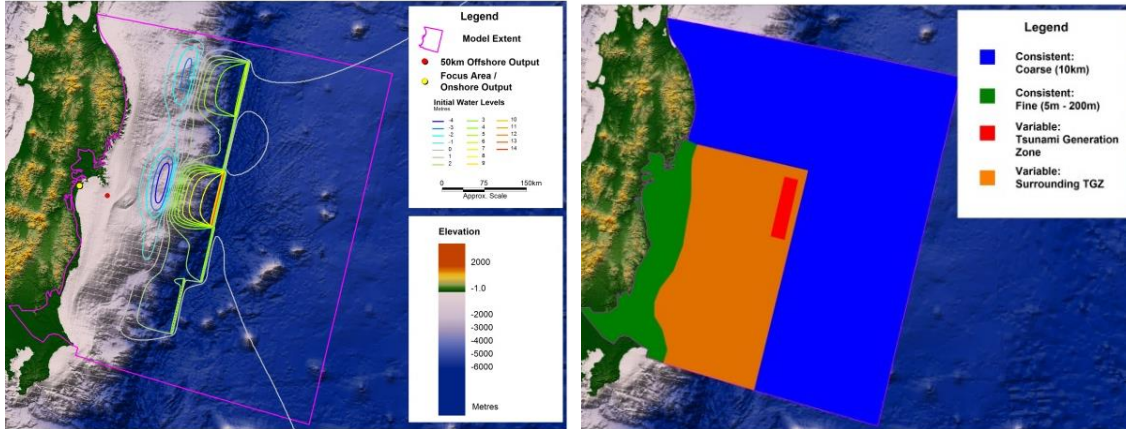


**Figure 6** Test site showing locality, model extent and initial water level condition (left) and model resolution zones (right).

**Table 2** Mesh resolution zones for sensitivity test runs (zone extents shown in Figure 6), total elements in mesh and model simulation times

Zone	Area (km <sup>2</sup> )	Simulation ID				
		1	2	3	4	5
Coarse	197,450	Consistent between simulations; mesh resolution 10km				
Fine	28,028	Consistent between simulations; mesh resolution 5-250m				
Variable - Tsunami Generation Zone	2,823	250	500	500	1000	1000
Variable - Surrounding TGZ	74,442	500	500	1000	1000	2000
Total Elements in Mesh		1,026,940	895,050	609,256	572,767	499,406
Model Run Time (hours, run on an Intel Xeon E5-2630 2.30GHz, 6 cores)	1st Order	2.16	1.54	0.94	0.82	0.74
	LCD Limiter	7.65	5.49	3.58	3.3	2.82
	MLG Limiter	11.88	8.7	5.66	5.23	4.45

Model results for each model simulation (3 spatial order simulations for each of the 5 mesh resolution simulations) are compared to 5 onshore locations where peak water level measurements were available (measurement locations and values shown in Figure 7, comparisons to model in Table 3). To demonstrate how the different spatial orders influence results, Figure 8 shows time series of water level variation at a location 50 km offshore and another onshore for the mesh resolution scenario 1 (the finest mesh resolution) and 5 (the coarsest mesh resolution).

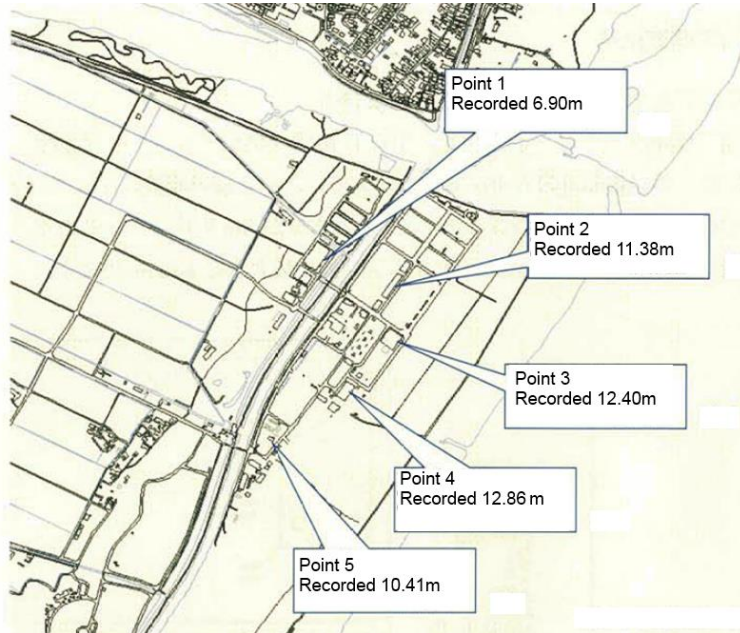


**Figure 7** Test site, showing locations and values of measured peak water level.

**Table 3** Comparison of model results with measured peak water levels (locations shown in Figure 7)

Mesh Resolution	Measurement Location 1, Recorded = 6.90m			Measurement Location 2, Recorded = 11.38m		
	Spatial Order			Spatial Order		
	1st Order	LCD Limiter	MLG Limiter	1st Order	LCD Limiter	MLG Limiter
1	6.05	7.35	8.63	8.98	11.32	11.66
2	6.04	7.28	8.59	9.03	11.25	11.60
3	5.78	7.12	8.58	8.38	11.00	11.87
4	5.72	7.09	8.53	8.25	10.93	11.75
5	5.08	6.72	8.40	7.14	10.65	12.02
Mesh Resolution	Measurement Location 3, Recorded = 12.40m			Measurement Location 4, Recorded = 12.86m		
	Spatial Order			Spatial Order		
	1st Order	LCD Limiter	MLG Limiter	1st Order	LCD Limiter	MLG Limiter
1	8.42	10.57	11.37	8.38	10.55	10.70
2	8.43	10.50	11.37	8.41	10.48	10.68
3	7.86	10.28	11.52	7.70	10.12	10.57
4	7.74	10.23	11.41	7.53	10.10	10.54
5	6.90	9.84	11.15	6.72	9.67	10.48
Mesh Resolution	Measurement Location 5, Recorded = 10.41m					
	Spatial Order					
	1st Order	LCD Limiter	MLG Limiter			
1	8.24	10.46	10.75			
2	8.24	10.40	10.71			
3	7.68	10.20	10.60			
4	7.53	10.13	10.59			
5	6.40	9.73	10.47			

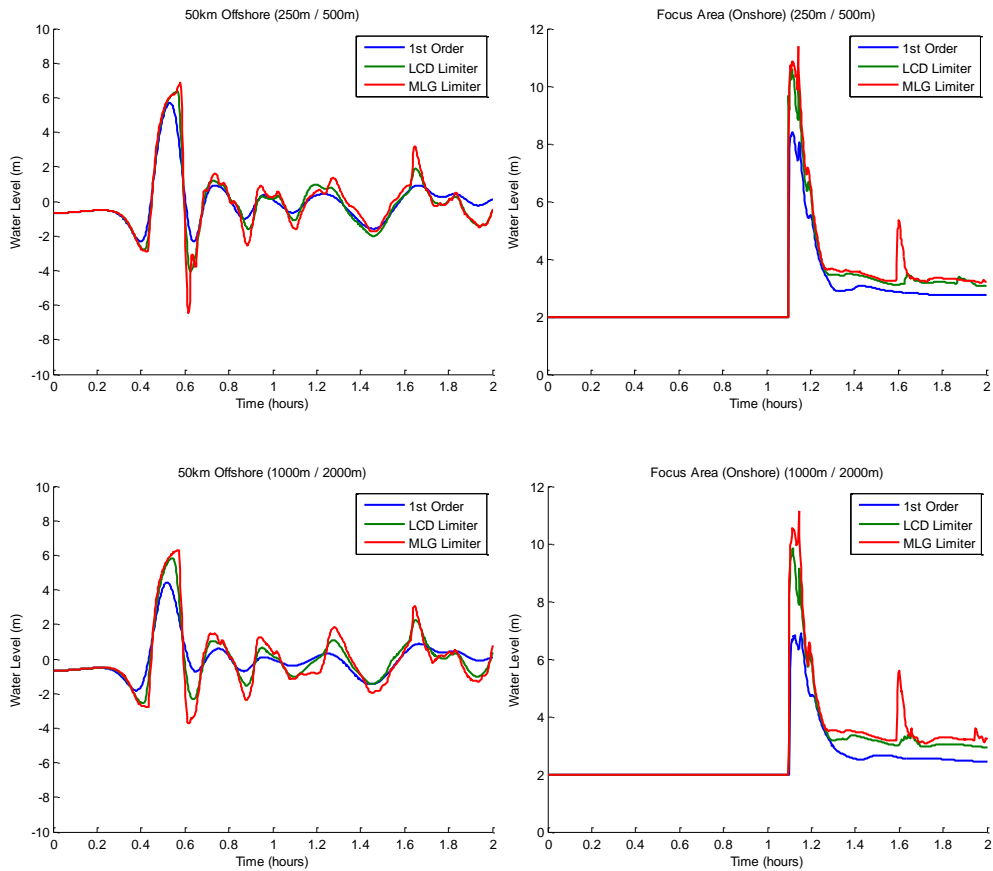


**Figure 8** Time series of water level for mesh resolution scenario 1 for the three spatial order scenarios at locations 50km offshore (left) and onshore(right) for fine resolution mesh scenario 1 (top) and coarse resolution mesh scenario 5 (bottom).

Model results are comparable to the measurements. Note that the measurement locations are around buildings and other urban infrastructure that may generate local complexities not represented in the model.

The rate of propagation of the tsunami wave from initial disturbance to arrival at the shoreline was insensitive to the spatial order and resolutions tested.

Model predictions of water level variation vary with differing mesh resolutions, especially when applying the first order spatial scheme. Sensitivity to mesh resolution tends to be less with the higher order spatial schemes. In all resolution scenarios the higher order schemes produce higher peak water levels, with the more compressive MLG limiter producing slightly higher peak water levels than the LCD limiter. This effect is amplified at the onshore areas with the second order schemes producing significantly higher peak water levels at all resolutions.

Both second order schemes produce sharper water level gradients on the wave fronts and demonstrate more high frequency fluctuations compared to the first order scheme. Both Figure 8 and Table 3 show that predicted peak water levels are higher for the second order schemes. Application of the MLG limiter, compared to the LCD limiter, further increases the sharp gradients, high frequency fluctuations and higher predicted peak water levels.

Figure 9 shows water level contours at a series of snapshots during the model simulation that demonstrate the tsunami wave propagation to the shoreline and subsequent overland inundation.

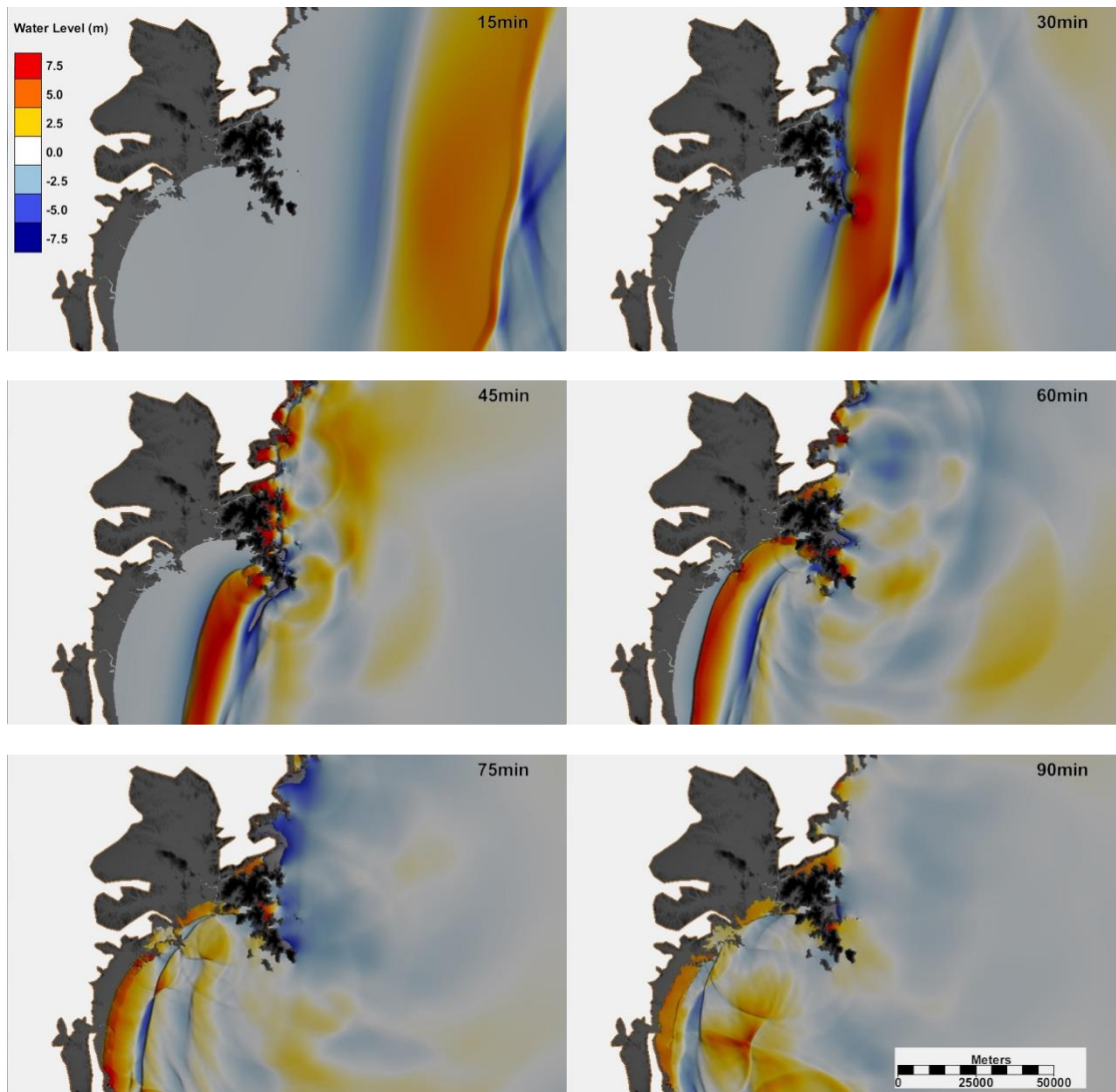


**Figure 9** Contours of water surface elevation of a sub-area of the model domain, showing tsunami propagation for mesh resolution scenario 1 and spatial order scenario 3 (second order MLG limiter) at outputs 15, 30, 45, 60, 75 and 90 minutes from simulation start.

#### 4 CONCLUSIONS

The three test cases investigated provide a progressive development of model application, from an analytical test to a physical model comparison to a “real world” application. The model demonstrates capability and accuracy; the combination of robust numerical scheme (which can handle steep gradients, high energy flow conditions and wetting and drying) with a flexible mesh approach (which can permit varying spatial resolutions to suit the application) is well suited to investigating the propagation of tsunami, from an initial water level state to shoreline and subsequent overland inundation. The third test case is a regional scale analysis with a mesh resolution of 5 to 10m at the shoreline that took several hours to complete on a standard desktop computer; this demonstrates the practical applicability of the modeling tool.

Choice of spatial discretization schemes in the numerical solution provides an opportunity to increase spatial accuracy within the same mesh, thus providing a more computationally efficient solution. The test cases suggest that application of a higher order spatial scheme tends to reduce sensitivity to mesh resolution in the results (however this may be a consequence of the range of mesh densities investigated).

Similar to the application of a higher order spatial scheme, a higher mesh density tends to improve the representation of the steep gradients that occur during tsunami propagation, and as such improves accuracy. However, results suggest for a given computational effort there is more gain in accuracy using a higher order spatial scheme compared to increasing mesh density. Thus, a higher order spatial discretization scheme is recommended for inclusion in simulations of tsunami propagation.

## ACKNOWLEDGEMENTS

This study is a contribution to a broader investigation. The authors would like to acknowledge the kind support and assistance of the following:

- Prof. Fujima of National Defense Academy of Japan
- Mr. Makoto Hada of FORUM8

## REFERENCES

- Batten, P., C. Lambert and D.M. Causon, 1996. Positively Conservative High-Resolution Convection Schemes for Unstructured Elements. *International Journal for Numerical Methods in Engineering*; 39, 1821-1838.
- BMT, 2013a. TUFLOW FV Science Manual. BMT WBM Pty Ltd, Brisbane, Queensland, 2013.
- BMT, 2013b. TUFLOWFV User Manual. BMT WBM Pty Ltd, Brisbane, Queensland, 2013.
- Carrier, G., T. Wu, and H. Yeh, 2003. Tsunami run-up and draw down on a sloping beach. *Journal of Fluid Mechanics*, 475, 79-99.
- Hubbard, M.E., 1999. Multidimensional Slope Limiters for MUSCL-Type Finite Volume Schemes on Unstructured Grids. *Journal of Computational Physics*, 155, 54-74.
- JIWET, 2013. The manual for application of tsunami numerical simulation model.
- Liu, P.L. F., Yeh, H. and Synolakis, C., 2008. Advanced Numerical Models for Simulating Tsunami Waves and Runup. *Advances in Coastal and Ocean Engineering*, 10, 250.
- Murillo, J., P. Garcia-Navarro, J. Burguete and P. Brufau, 2006. A conservative 2D model of inundation flow with solute transport over dry bed. *International Journal for Numerical Methods in Fluids*; 52, 1059-1092.
- Murillo, J., P. Garcia-Navarro, J. Burguete and P. Brufau, 2007. The influence of source terms on stability, accuracy and conservation in two-dimensional shallow flow simulation using triangular finite volumes. *International Journal for Numerical Methods in Fluids*; 54, 543-590.
- Pope, S.B., 2000. *Turbulent Flows*. Cambridge University Press.
- Roe, P.L., 1981. Approximate Riemann solvers, parameter vectors and difference schemes. *Journal of Computational Physics*, 43, 357-372.
- Synolakis, C.E., Bernard, E.N., Titov, V.V., K anođlu, U. and Gonz alez, F.I., 2007. Standards, criteria, and procedures for NOAA evaluation of tsunami numerical models. NOAA Tech. Memo. OAR PMEL-135, NOAA/Pacific Marine Environmental Laboratory, Seattle, WA, 55.
- XP Solutions, 2013. *xpswmm2D User Manual*. XP Solutions, Inc., Portland, OR, 2013.